

Neutron Resonance Transmission Analysis with a Compact Deuterium-Tritium Neutron Generator

Ethan A. Klein, Farheen Naqvi, Jacob E. Bickus, Hin Y. Lee, and Areg Danagoulian*
Department of Nuclear Science and Engineering, MIT, Cambridge, MA 02139, USA

Robert J. Goldston
Princeton Plasma Physics Laboratory, Princeton NJ 08543, USA
 (Dated: April 10, 2022)

Neutron Resonance Transmission Analysis (NRTA) is a spectroscopic technique which uses the resonant absorption of neutrons in the epithermal range to infer the isotopic composition of an object. This spectroscopic technique has relevance in many traditional fields of science and nuclear security. NRTA in the past made use of large, expensive accelerator facilities to achieve precise neutron beams, significantly limiting its applicability. In this work we describe a series of NRTA experiments where we use a compact, low-cost deuterium-tritium (DT) neutron generator to produce short neutron beams (2.6 m) along with a ^6Li -glass neutron detector. The time-of-flight spectral data from five elements – silver, cadmium, tungsten, indium, and ^{238}U – clearly show the corresponding absorption lines in the 1-30 eV range. The experiments show the applicability of NRTA in this simplified configuration, and prove the feasibility of this compact and low-cost approach. This could significantly broaden the applicability of NRTA, and make it practical and applicable in many fields, such as material science, nuclear engineering, and arms control.

I. INTRODUCTION

Most isotopes exhibit resonance behavior when interacting with neutrons. Some of the elements – many of them with mid and high atomic number Z – undergo resonance scattering, absorption, and fission in the epithermal 1-100 eV regime. In this energy range the resonances are sufficiently narrow and well separated that a given set of observed resonances constitutes a unique identifier of a particular isotope. Thus, spectroscopic measurement of neutron transmission and the resulting observation of attenuation dips in the transmitted spectrum can be used to infer the isotopic and elemental content of an unknown target. This is the basis of neutron resonance transmission analysis (NRTA).

In the past NRTA has found applications in fields as broad as nuclear engineering, nuclear physics, and archaeology [1–11]. Furthermore, past work in arms control has demonstrated the applicability of NRTA for problems of treaty verification [12, 13]. These applications have exploited the isotopic specificity of the NRTA signal, as measured using pulsed neutron beams and time-of-flight (TOF) techniques. These applications have been limited by their use of major facilities and kilometer-long accelerators. This circumstance has been a significant limitation to the broad applicability of an otherwise very powerful methodology. Recent work has been done with the goal of reducing size by employing accelerator-based neutron sources towards NRTA implementations [14–16], however even these involve fairly large experimental facilities.

In this experimental study we demonstrate that this technique can be significantly improved by making it ubiquitous through the use of relatively cheap, compact, and commercially available pulsed DT neutron sources when combined with short (2.6 meters-long) neutron beamlines. This effort requires a careful optimization of the moderator assembly and

shielding – to maximize the output in the 1-100 eV range and to reduce otherwise large neutron scatter and neutron capture backgrounds. Our past work via Monte Carlo (MC) simulations has indicated that such an approach is feasible [17]. NRTA applications using compact neutron sources can be further enhanced by using the results from ongoing research into high intensity, pulsed DT and deuterium-deuterium (DD) neutron sources [18, 19].

II. BACKGROUND

The NRTA technique involves analysis of the magnitude and energy of absorption lines in neutron transmission spectra to reconstruct the isotopic composition of a target object. In combination with evaluated neutron cross section data, the transmission spectrum can be used to estimate the linear density of the different isotopes present in the target object [8].

For a neutron beam impinging on an unknown target material, total cross section is a combination of both elastic potential scattering, which is nearly independent of energy, and resonant interactions [20]. At the resonance energies, the enhanced cross section of forming a compound nucleus in a particular excited state can be approximated by the single-level Breit Wigner formalism [20]. The cross section for compound nuclear formation by entrance channel α and subsequent reaction by exit channel β , $\sigma_{\alpha\beta}$, is given by

$$\sigma_{\alpha\beta} = \frac{\pi}{k^2} \frac{\Gamma_{\alpha}\Gamma_{\beta}}{(E - E_{\text{res}})^2 + (\Gamma/2)^2}, \quad (1)$$

where Γ is the total decay width, Γ_{α} and Γ_{β} are the partial widths for the entrance channel α and exit channel β , respectively, k is the wavenumber, and E_{res} is the resonant energy [21]. At energies of 1-100 eV the predominant resonant interaction is (n, γ) , resulting in absorption of the incoming neutron and observation of a dip in the neutron transmission spectrum.

* aregian@mit.edu

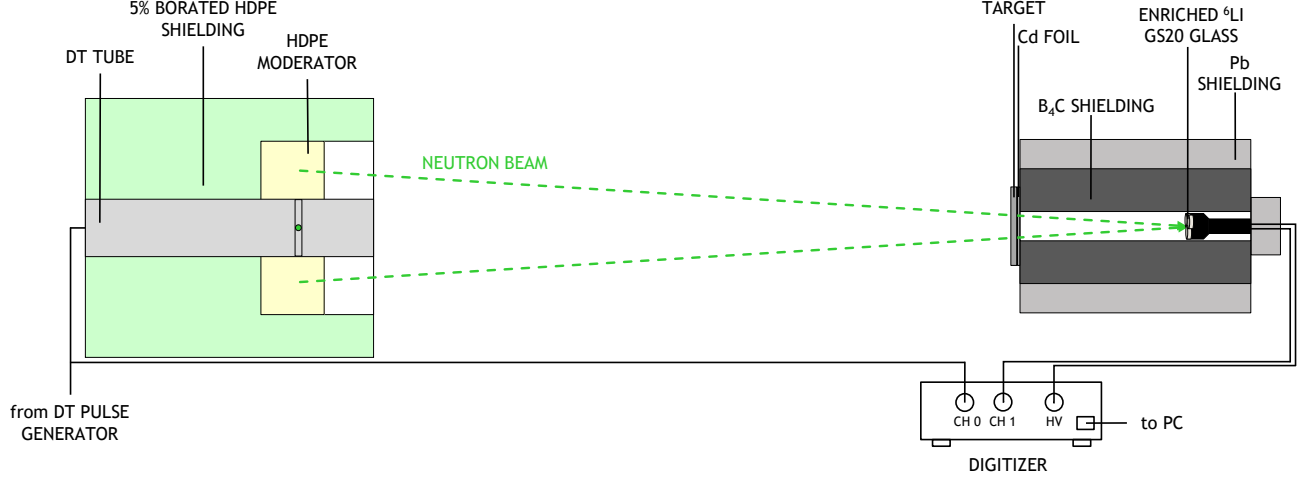


FIG. 1. Schematic of the experimental setup. The DT neutron generator is shielded by a box of borated plastic with a radial moderator composed of high-density polyethylene. The moderated neutron beam is incident on a target and detected in a 1" thick GS20 enriched ${}^6\text{Li}$ glass scintillator, shielded from neutrons by boron carbide and from photons by lead. Thermal wraparound neutrons are filtered by 3.0 mm of cadmium foil placed along the axis.

Neutron transmission through a homogeneous target at a given incident energy, $T(E_n)$, will depend on the identities and areal densities of the isotopes present in the target, and can be written as

$$T(E_n) = \frac{I(E_n)}{I_0(E_n)} = \exp\left(-\sum_i \sum_j n_i \sigma_{i,j}(E_n) \Delta x_i\right), \quad (2)$$

where $I(E_n)$ and $I_0(E_n)$ are the neutron fluxes measured at the detector for target and open beam runs, respectively, n_i is the atomic number density for isotope i , Δx_i is the target thickness for isotope i , and $\sigma_{i,j}(E_n)$ is the interaction cross section for isotope i and reaction j . Since the resonance energies and amplitudes are characteristic of the isotopes present in the target, the neutron transmission spectrum will be unique for a given target isotopic composition, making it an isotopic-geometric signature of a particular fissionable object, as described in Ref. [13]. Although some isotopes have individual resonances sufficiently close to those of another isotope that the two cannot be distinguished, in most cases the combination of their multiple resonances can enable isotopic differentiation.

Unlike traditional gamma spectroscopy, which is only sensitive to unstable isotopes, NRTA can characterise any stable isotope which has sufficiently strong and well-resolved resonances in the neutron energy region of interest. It can also provide geometric information by using a position-sensitive detector [22–24], otherwise difficult with gamma spectroscopy. This advantage is particularly important in arms control applications [25] and is supported by the fact that many isotopes of interest to nuclear security (*e.g.* ${}^{235}\text{U}$, ${}^{238}\text{U}$, ${}^{239}\text{Pu}$, ${}^{240}\text{Pu}$) exhibit (n,γ) and $(n,\text{fission})$ neutron resonances in the epithermal energy region (1–100 eV). The capability of NRTA to perform isotopic identification and quantification will be limited by the thickness of the target and the presence of any shielding.

III. EXPERIMENTAL TECHNIQUE

A. Experimental Setup

The experiments were performed at the Vault Laboratory for Nuclear Science at MIT. A schematic diagram of the experimental setup is shown in Fig. 1. The neutron source was a portable A320 DT neutron generator, manufactured by Thermo Fisher Scientific Inc., that nominally generates $\sim 1 \times 10^8$ neutrons per second. The neutron generator was operated at 5 kHz repetition rate and 5% nominal duty factor with an acceleration voltage of 90 kV. Although the nominal pulse width is 10 μs , due to voltage rise times and plasma formation time scales, the actual neutron pulse is only $\sim 3.3 \mu\text{s}$ long after a $\sim 7 \mu\text{s}$ delay (see inlay of Fig. 2). These neutrons are produced nearly isotropically through the ${}^3\text{H}({}^2\text{H},n){}^4\text{He}$ fusion reaction, with neutron energies of 14.1 MeV in the direction of the moderator. To moderate the emitted neutrons to the epithermal energy range, a 10.0 cm thick, radial high-density polyethylene (HDPE) hollow cylinder moderator was placed around the DT tube. Surrounding the moderated source was 5% borated polyethylene shielding to reduce neutron and gamma backgrounds.

All experiments discussed in this paper used a distance of 2.62 m from the tritium target in the DT tube to the front face of the detector. The detector setup consisted of three adjacent $25.4 \text{ mm} \times 5 \text{ mm}$ disks of ${}^6\text{Li}$ -enriched GS20 scintillator glass optically mounted on a 6.4 cm diameter photomultiplier tube (PMT) operated at 1150 V [26]. The detector and PMT were placed within an aluminum box filled with boron carbide B_4C powder for thermal and epithermal neutron shielding, with a collimated opening in the front. The box was surrounded by 2" thick lead shielding. Neutrons were detected in the GS20

glass via the ${}^6\text{Li}(n, {}^3\text{H}){}^4\text{He}$ reaction, depositing 4.78 MeV in the detector. This corresponds to the light output of approximately 1.6 MeVee [27]. The DT pulse initiation signal and the PMT were read into two channels of a CAEN V1725 14-bit digitizer, which samples at the rate of 250 MS/s. Data acquisition was handled by the ADAQ toolkit [28] and data were analyzed using both ROOT [29] and the SciPy [30] and ImagingReso [31] Python libraries.

B. Background Reduction

Accurately measuring the neutron transmission requires reducing the large backgrounds in the form of photons and unwanted neutron scattering within the detector assembly. The main source of γ background is the ${}^1\text{H}(n, \gamma){}^2\text{H}$ reaction in the moderator surrounding the DT source, producing 2.2 MeV photons which are detected on the time-frame of neutron thermalization in the moderator (~ 10 s of μs). The digital signal analysis method of charge integration had previously been shown to improve neutron gamma discrimination in PMT response from GS20 scintillators by a factor of over 60 compared to pulse height analysis [32], and so was chosen in this study to preferentially select neutron counts. To further reduce the photon contributions, the thickness of the GS20 scintillator glass was chosen to be 5 mm. Another considerable background contribution to the detection of epithermal neutrons are the wraparound neutrons (*i.e.* slower neutrons incident on the detector during a subsequent pulse window). These however can be significantly reduced by the use of a cadmium filter, as discussed later.

Surrounding the detector with 2.5-4 cm of boron carbide powder reduced the thermal neutron background by almost 99%. The impact of wraparound neutrons was minimized by a combination of a 200 μs pulse repetition period and the placement of 3.0 mm Cd foil on-axis in front of the detector assembly. For the given pulse repetition rate and a distance of 2.62 m between the moderator assembly and the detector, only neutrons with energies ~ 0.75 eV and below could result in wraparound. The (n, γ) cross section of ${}^{113}\text{Cd}$, a naturally occurring isotope, has a major, broad resonance at 0.17 eV of 10 kb which makes it an efficient material to absorb neutrons with energy below the ~ 0.75 eV cutoff. The utility of NRTA is not affected much by the presence of the Cd foil as very few isotopes have resonances below this cutoff (*e.g.* ${}^{176}\text{Lu}$, ${}^{151}\text{Eu}$, ${}^{191}\text{Ir}$) and epithermal neutron attenuation at higher energies due to 3.0 mm Cd is only $\sim 1\%$.

C. Time-of-Flight (TOF) Measurement

NRTA requires measurement of neutron energy in order to reconstruct the neutron transmission as a function of incident neutron energy. In these experiments, measurements of neutron TOF were used to reconstruct neutron energy. For a defined TOF path length d_{TOF} , the following non-relativistic, kinematic relationship can be used to infer the neutron energy,

E_n :

$$E_n = \frac{1}{2} m_n \left(\frac{d_{\text{TOF}}}{t_{\text{TOF}}} \right)^2 \quad (3)$$

where m_n is the neutron mass and $t_{\text{TOF}} = t_{\text{signal}} - t_{\text{pulse}}$. Here t_{signal} is the time of the detector trigger and t_{pulse} is the center time of the neutron generation pulse. The resulting uncertainty in neutron energy is given by,

$$\frac{\delta E_n}{E_n} = 2 \sqrt{\left(\frac{\delta t_{\text{TOF}}}{t_{\text{TOF}}} \right)^2 + \left(\frac{\delta d_{\text{TOF}}}{d_{\text{TOF}}} \right)^2} \quad (4)$$

where d_{TOF} is the TOF distance, δd_{TOF} is the uncertainty in TOF distance, and δt_{TOF} is the uncertainty in TOF [33]. It is clear from this expression that for $\sim \text{eV}$ low energy neutrons (*i.e.* large t_{TOF}) the uncertainty in energy reconstruction is primarily driven by uncertainties in d_{TOF} , δd_{TOF} . On the other hand for the higher energy neutrons > 10 eV the energy uncertainty is dominated by contributions from δt_{TOF} . Thus, neutron sources with narrower pulses would be necessary in order to access absorption lines at energies much higher than 25 eV.

The uncertainty in TOF, δt_{TOF} , has contributions from the DT pulse width and the time resolution of the detector, which for a ${}^6\text{Li}$ glass scintillator detector is typically ~ 60 ns [32]. Uncertainty in moderation time distribution is instead treated in the spatial uncertainty, which GEANT4 simulations showed to increase nonlinearly as the moderated neutron energy decreases. The main source of uncertainty in time of flight for this setup is thus due to the width of the DT pulse. For these experiments, the DT generator was set to produce a 10 μs pulse, the minimum pulse width possible for the A320 DT generator. As discussed earlier, due to the plasma dynamics and neutron generation in the DT source [34], the actual width observed in neutron production was $\sigma = 1.41 \pm 0.06 \mu\text{s}$.

The uncertainty in TOF distance is a result of the spatial spread of the neutrons following moderation from 14.1 MeV to epithermal energies. To minimize the impact of δd_{TOF} , longer flight distances are preferred but the need for practical measurement times, due to reduction in neutron flux with distance, sets a limit on the latter. A distance of 2.62 m, between the front face of the detector and the tritium disk within the DT tube, was thus chosen to support an acceptable TOF resolution while maintaining feasible measurement times. This distance is greater than the TOF distance as it does not account for neutron moderation, and a best fit to experimental data determined the effective d_{TOF} to be 2.57 m. The flight time of ~ 1 eV neutrons is on the order of 185 μs for this distance, within the period of the DT neutron generator.

D. Data Acquisition & Processing

The data was acquired in a list mode, with one channel reading the signal pulses from the PMT coupled to the detector, while the other channel read the TTL pulses from the DT generator's driving circuitry. In the post-processing, each

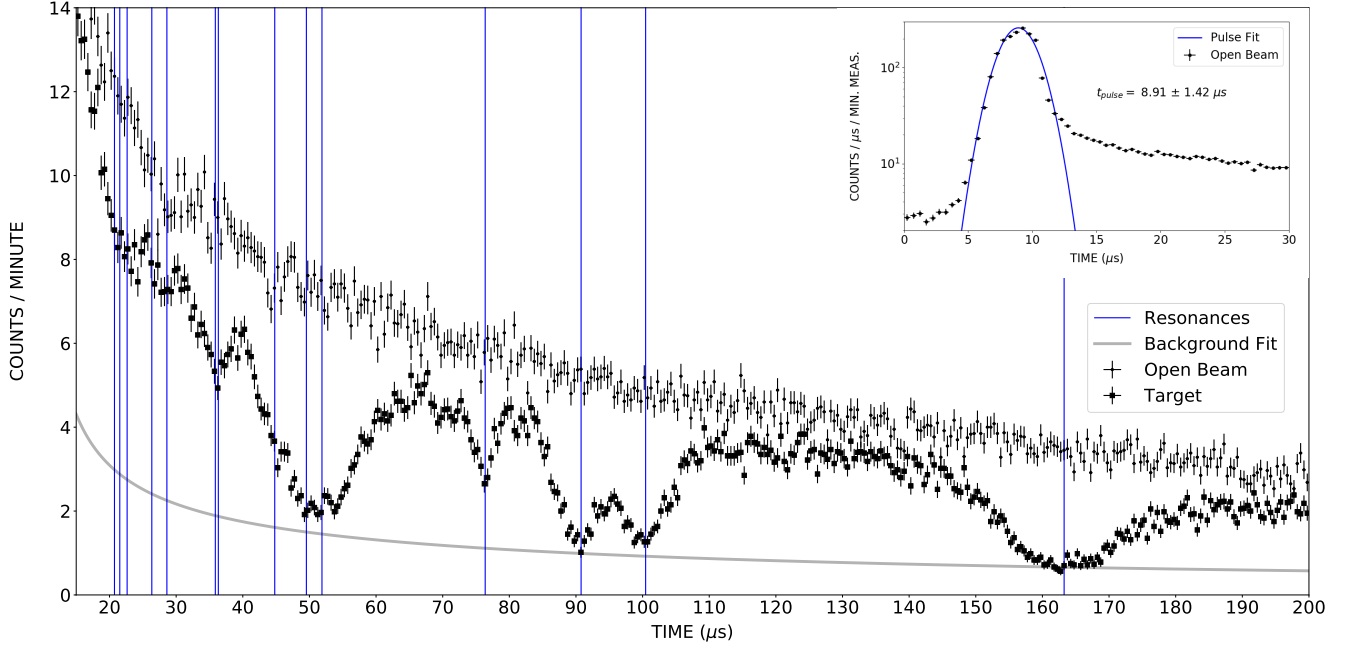


FIG. 2. TOF distribution for a 2-hour run with a 6.9mm-thick composite target containing W, Ag, Cd, and In. The background fit, shown in grey was performed according to the method discussed in Section IV A. The location of the expected resonance energies (blue lines) matches the location of the observed attenuation lines. The inlay plots the total range, showing the main DT pulse at $\sim 8.9 \mu\text{s}$ with a width of $\sigma = 1.4 \mu\text{s}$.

detector pulse was associated with a preceding TTL pulse and the TOF was calculated. As both channels used ADCs driven by the same 250 MHz clock this allowed for determination of signal time with the electronic precision of 4 ns. In addition to the TOF determination it was necessary to further filter the data to reduce the γ backgrounds that were present due to the sensitivity of the GS20 scintillator to photons. By integrating the pulse area a quantity proportional to the light output of the scintillator was computed. The light output distribution was then analyzed to identify the main neutron peak due to the light output from alphas and tritons produced in the ${}^6\text{Li}(n,\alpha){}^3\text{He}$ reaction in the scintillator. A Gaussian fit was performed, and a $\pm 2\sigma$ cut was placed, thus significantly reducing the photon background. With the Cd filter in front and no target present, a DAQ trigger rate of $< 200 \text{ s}^{-1}$ was observed in the ${}^6\text{Li}$ detector.

IV. RESULTS & ANALYSIS

Experimental measurements ranging from 10 minute to 2 hour runs were performed for various target compositions of W, Ag, In, and ${}^{238}\text{U}$ ranging in thickness from 0.25 mm to 3.5 mm. The raw counts within the neutron cut described in the previous section were normalized to counts per minute and binned with $0.5 \mu\text{s}$ bin width. Fig. 2 shows an example plot of a target consisting of In, W, and Ag in addition to the Cd filter foil, along with the corresponding resonance energies from ENDF/B-VIII.0 libraries plotted as vertical lines [35]. Distinct absorption lines for indium, tungsten, and silver isotopes

are clearly observable, as well as Cd lines in the open beam spectrum, allowing for subsequent element identification analysis. As part of future work the absolute concentrations of the isotopes can be further extracted from this data — a goal that is particularly important for arms control applications where the enrichment of a fissile material is of importance.

A. Background Correction

The background reduction methods described in III B, in addition to the detector pulse integral cut, eliminated most of the unwanted photon and scattered neutron counts from the TOF spectrum. However, some residual background was present in the data, as observed at the bottoms of attenuation lines that should have had no counts due to very high cross sections. Therefore an additional correction function was applied to the data to estimate and subtract the residual background.

The background was modeled using the "black resonance" technique where a strongly resonant target (e.g. tungsten, silver, indium) is placed in the beam path and the background function is fit to the bottom of the "saturated" absorption lines. This technique is described in detail by Syme *et al.* in Ref. [36]. A function of the following form was used following Fei *et al.* [10]:

$$B(t_m) = b_0 + b_1 e^{-t_m/\tau_1} + b_2 t_m^{-\tau_2} \quad (5)$$

where t_m is the neutron detection time corrected for the median pulse time, and b_0 , b_1 , b_2 , τ_1 , and τ_2 are fitting parameters.

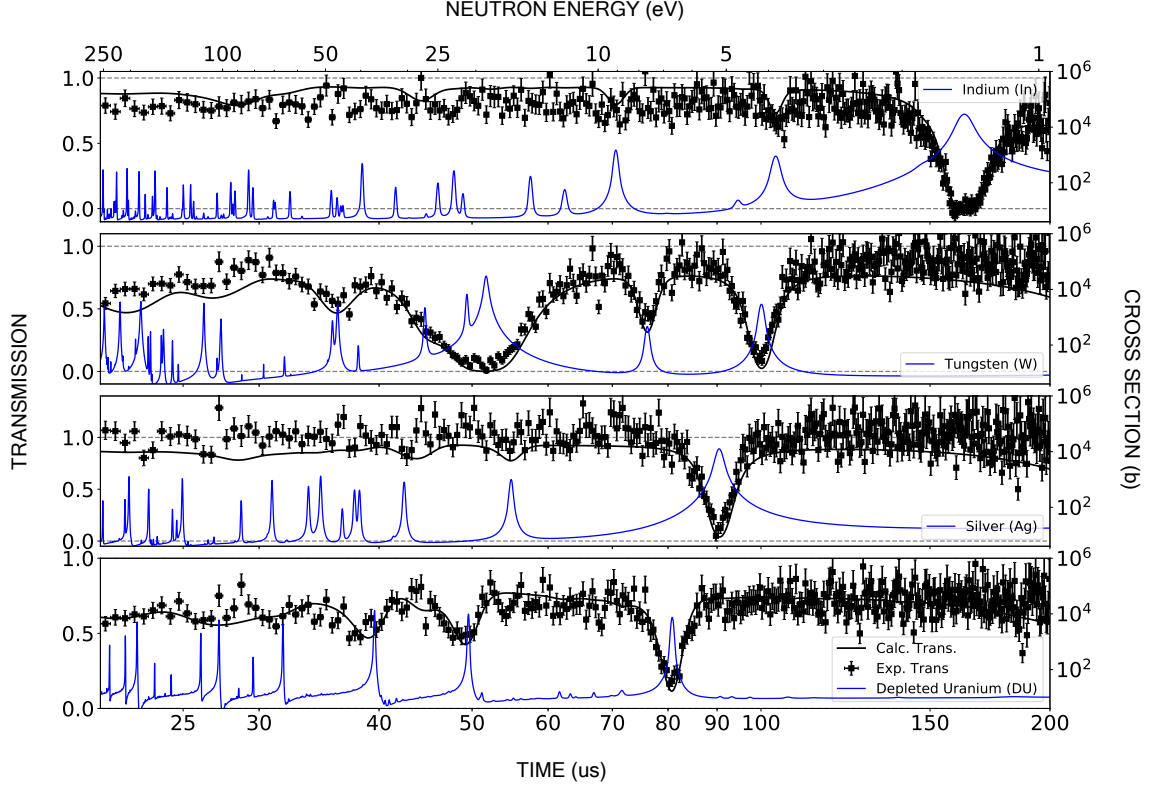


FIG. 3. Neutron cross section and transmission data as shown for single element targets (Top-to-bottom: In, W, Ag, ^{238}U). Experimental data is plotted along with the calculated transmission, which uses ENDF-VIII.0 evaluated neutron cross section data convolved with the DT pulse width. Horizontal dotted lines demarcate zero transmission ($T=0$) and total transmission ($T=1$). The $\sim 10\%$ discrepancies are likely due to the limitations of the empirical model used for background subtraction.

ters. The first term in Eq. 5 accounts for constant background, the second accounts for the TOF distribution of 2.2 MeV γ from neutron capture on ^1H , and the third accounts for the background due to neutrons that underwent elastic scattering within the detector assembly before detection.

This function was fit to the resonance lines of In (1.46 eV), W (4.15 eV, 18.84 eV), and Ag (5.19 eV) in data from a dedicated 2-hour run. To quantify the contributions of 2.2 MeV photons, separate dedicated experiments were performed involving target-in and target-out runs using a LaBr_3 detector. A decay constant of $\tau_1 = 75 \pm 3 \mu\text{s}$ was extracted using the LaBr_3 data, and was used as a bound to the fit described by Eq. 5. With τ_1 thus determined, the neutron data was then fitted with Eq. 5 to determine the other parameters.

In applying the fit, attenuation of the 2.2 MeV photon background component in the target must be taken into account. Photon attenuation in each target was calculated using the number densities and mass attenuation coefficients [37] for each element present in the target and the ratio was taken to the attenuation in the "black resonance" target used for the background fit. This correction was not applied to the neutron component of the target given the assumption that in-scatter of neutrons in the detector assembly would be independent of target thickness, which was evidenced by statistical analysis of the best fit. Fig. 2 shows the obtained fit function providing

an estimate of the energy dependent background counts that were then subtracted from the experimental data.

B. NRTA of Single-Element Targets

Targets composed of a single mid- or high-Z material sheet with strong neutron resonances were analyzed to measure the capability of the system to resolve resonances of varying widths across the epithermal energy range. The TOF histograms for target-in and open beam measurements were first background corrected using the process described above. Then neutron transmission through the target was calculated by dividing the target-in histogram by the target-out histogram. Fig. 3 shows the background-corrected neutron transmission for single element targets and plots the elemental neutron cross section for comparison. The transmission was also computed by convolution of ENDF/B-VIII.0 cross section data with the DT neutron pulse shape, and is overlaid as the black line in the plot [35].

Neutron resonances of sufficient width can be identified up to 50 eV. Although this upper energy bound is much lower than that of fixed facility NRTA setups, which can identify resonances up to the keV range, the neutron transmission through each element presented here is clearly identifiable

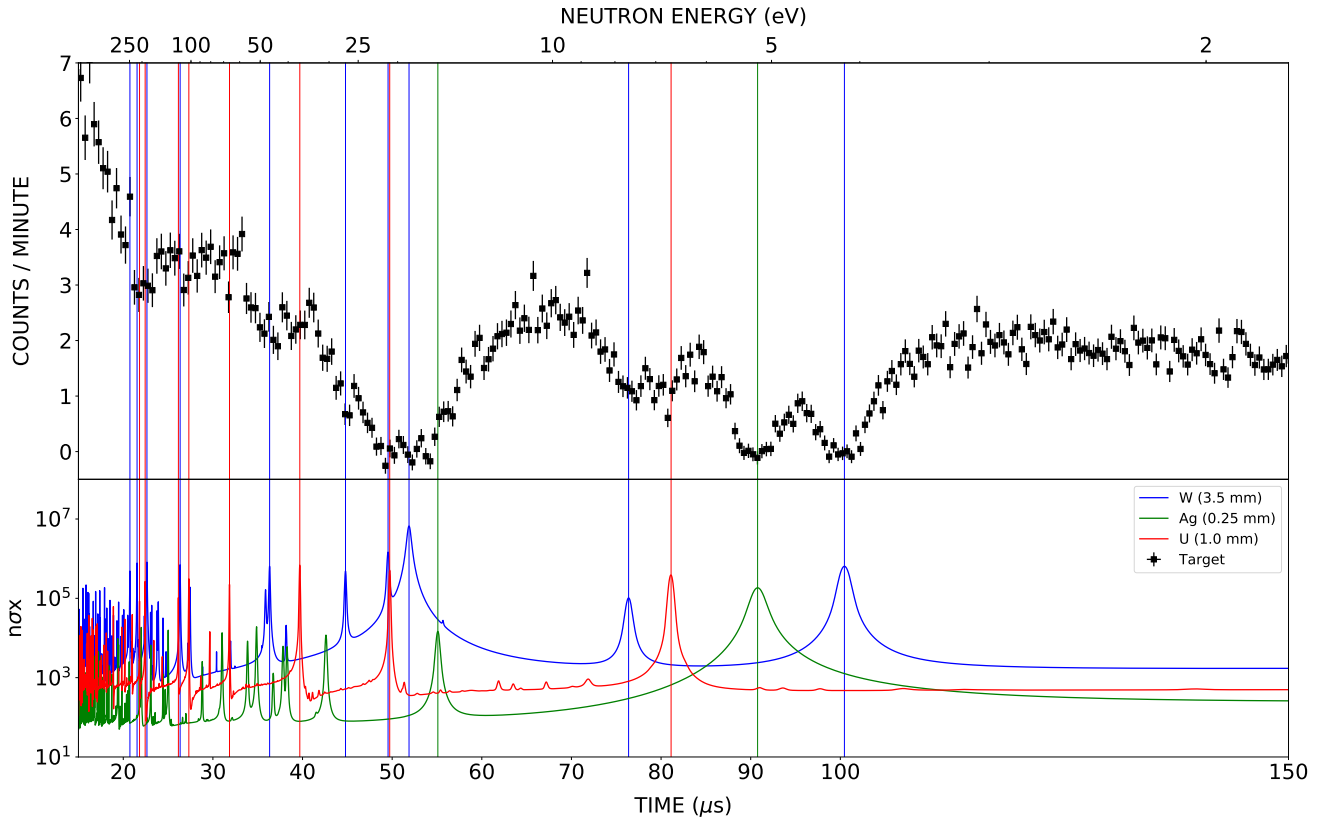


FIG. 4. Plot of background-corrected transmitted neutron counts for a 2-hour run with an 8.9mm-thick target containing W, Ag, U, Pb, and Cd. The products for each element's total neutron cross section with its number density and elemental thickness are plotted beneath. At low incident neutron energies resonances within 1.0 eV are well resolved.

and matches the calculated transmission, demonstrating sufficiency for isotopic identification applications. For nuclear security and safeguards applications, ^{238}U resonances at 6.7 eV, 20.9 eV, and 36.7 eV are well resolved and thus can be used to indicate the presence of ^{238}U in the target.

The value of the reconstructed transmission is heavily dependent on the choice of background fit parameters. While achieving a good overall agreement, it can also be seen to diverge from the calculated transmission in non-resonant regions in some cases by approximately 10%. This will not have an effect on elemental detection and attribution as that goal primarily depends on the observation of resonant dips. This however could effect quantification of elemental concentration in the target as it relies on the magnitude of the attenuation in the dip to that between the resonances to determine isotopic number densities. Thus future work should focus on better understanding and modeling of the backgrounds, *e.g.* via detailed Monte Carlo simulations, which would allow for a more precise determination of the transmission and more accurate estimations of isotopic concentrations in the target.

C. NRTA of Composite Targets

Isotopic identification of multi-elemental targets requires the ability to differentiate individual resonances. Fig. 4 shows

the background-subtracted transmission for a 2-hour run with a composite target of W, Ag, Pb, and depleted uranium (99.9% ^{238}U) foils (in addition to the fixed Cd foil). As can be seen from comparison to the elemental neutron cross sections, all resonances below 20 eV can be attributed to individual elements, whereas higher energy resonances are observed but due to their close spacing are not always attributable to specific elements. The spacing between the 20.9 eV resonance of ^{238}U and the 18.8 eV ^{186}W and 21.1 eV ^{182}W resonances is too close to resolve with the 3.3 μs wide pulse of the DT generator. For that reason, nuclear security applications requiring identification of ^{238}U presence in a target will have to rely on measuring the 6.7 eV ^{238}U resonance if tungsten is present, unless longer measurement times or narrower DT pulses such as those achievable by a P235 generator are used [38].

V. CONCLUSION

In this work we have shown the feasibility of performing NRTA measurements using a compact DT generator and short, ~ 2.6 m neutron TOF beamlines, and involving measurement times of approximately 2 hrs. The measurements were able to observe the resonant (n,n) elastic scattering and (n, γ) absorption lines in the 1-30 eV range from elements of a broad range of Z. This compact and economic configura-

tion can significantly increase the applicability of a powerful technique which in the past has been extremely limited due to the necessity of large accelerators and long neutron beam-lines. This in its turn would allow for practical applications in such fields as materials analysis, archaeology, and nuclear engineering. Verification of arms control treaties in particular would benefit significantly from the use of such compact platforms in combination with already-proven NRTA methods as described in Ref. [12, 13].

In its current form the technique does have a number of limitations and would benefit from the following future improvements. The TOF resolution is limited by the $\sim 1.4 \mu\text{s}$ DT pulse, which reduces the ability to resolve absorption lines above 50 eV. The pulse can be shortened either by modifying the DT operation, or using more advanced, faster pulsed neutron sources such as those described in Ref. [18, 38]. This is of particular importance when it comes to elements whose powerful resonances below 50 eV result in the saturation of the absorption lines: to quantify the isotopic concentrations one would need to observe and quantify the weaker, higher energy resonances. The technique is also limited by the presence of

residual photon backgrounds from (n, γ) neutron capture inside the moderator. While energy-based filtering and background corrections have been effective, the sensitivity could be further improved by using detectors with a higher ability to discriminate between neutron and photon hits. For example, CLYC detectors appear promising in this regard [39, 40]. Finally, these measurements would benefit from a more powerful pulsed neutron source, allowing for better statistics and shorter measurement times. Research is currently underway to develop such sources [19, 41].

VI. ACKNOWLEDGEMENTS

This work was supported in part by Department of Energy Award No. DE-NA0003920, as part of the NNSA Consortium of Monitoring, Technology, and Verification (MTV). The authors would like to thank their colleagues in MTV and MIT's Department of Nuclear Science and Engineering for encouragement and advice.

-
- [1] D. L. Chichester and J. W. Sterbentz, Assessing the feasibility of using neutron resonance transmission analysis (NRTA) for assaying plutonium in spent fuel assemblies, *Journal of Nuclear Materials Management* **XL** (2012).
 - [2] M. A. Bourke, S. C. Vogel, S. L. Voit, K. J. McClellan, A. S. Losko, and A. Tremsin, *Non destructive examination of UN/U-Si fuel pellets using neutrons (preliminary assessment)*, Tech. Rep. (Los Alamos National Lab.(LANL), Los Alamos, NM (United States), 2016).
 - [3] P. Schillebeeckx, B. Becker, H. Harada, and S. Kopecky, Neutron resonance spectroscopy for the characterization of materials and objects, in *Supplement to Volume I/24* (Springer, 2015) pp. 10–66.
 - [4] C. Andreani, G. Gorini, and T. Materna, Novel neutron imaging techniques for cultural heritage objects, in *Neutron Imaging and Applications* (Springer, 2009) pp. 229–252.
 - [5] J. W. Sterbentz and D. L. Chichester, *Neutron Resonance Transmission Analysis (NRTA): A Nondestructive Assay Technique for the Next Generation Safeguards Initiative's Plutonium Assay Challenge*, Tech. Rep. (Idaho National Laboratory, 2010).
 - [6] A. Tremsin, S. Vogel, M. Mocko, M. Bourke, V. Yuan, R. Nelson, D. Brown, and W. Feller, Non-destructive studies of fuel pellets by neutron resonance absorption radiography and thermal neutron radiography, *Journal of Nuclear Materials* **440**, 633 (2013).
 - [7] G. Festa, E. P. Cippo, D. Di Martino, R. Cattaneo, R. Senesi, C. Andreani, E. Schooneveld, W. Kockelmann, N. Rhodes, A. Scherillo, P. Kudejova, K. Biro, K. Duzs, Z. Hajnal, and G. Gorini, Neutron resonance transmission imaging for 3D elemental mapping at the ISIS spallation neutron source, *Journal of Analytical Atomic Spectrometry* **30**, 745 (2015).
 - [8] H. Hasemi, M. Harada, T. Kai, T. Shinohara, M. Ooi, H. Sato, K. Kino, M. Segawa, T. Kamiyama, and Y. Kiyonagi, Evaluation of nuclide density by neutron resonance transmission at the noboru instrument in j-parc/mlf, *Nuclear Instruments and Methods in Physics Research Section A: Accelerators, Spectrometers, Detectors and Associated Equipment* **773**, 137 (2015).
 - [9] C. Paradela, J. Heyse, S. Kopecky, P. Schillebeeckx, H. Harada, F. Kitatani, M. Koizumi, and H. Tsuchiya, Neutron resonance analysis for nuclear safeguards and security applications, in *EPJ Web of Conferences*, Vol. 146 (EDP Sciences, 2017) p. 9002.
 - [10] F. Ma, S. Kopecky, G. Alaerts, H. Harada, J. Heyse, F. Kitatani, G. Noguere, C. Paradela, L. Šalamon, P. Schillebeeckx, H. Tsuchiya, and R. Wynants, Non-destructive analysis of samples with a complex geometry by NRTA, *J. Anal. At. Spectrom.* **35**, 478 (2020).
 - [11] G. Noguere, F. Cserpak, C. Ingelbrecht, A. Plompen, C. Quetel, and P. Schillebeeckx, Non-destructive analysis of materials by neutron resonance transmission, *Nuclear Instruments and Methods in Physics Research Section A: Accelerators, Spectrometers, Detectors and Associated Equipment* **575**, 476 (2007).
 - [12] J. J. Hecla and A. Danagoulian, Nuclear disarmament verification via resonant phenomena, *Nature Communications* **9**, 1259 (2018).
 - [13] E. M. Engel and A. Danagoulian, A physically cryptographic warhead verification system using neutron induced nuclear resonances, *Nature Communications* **10**, 4433 (2019).
 - [14] H. TSUCHIYA, F. KITATANI, M. MAEDA, Y. TOH, and M. KURETA, Development of Neutron Resonance Transmission Analysis as a Non-Destructive Assay Technique for Nuclear Nonproliferation, *Plasma and Fusion Research* **13**, 2406004 (2018).
 - [15] H. Harada, F. Kitatani, M. Koizumi, J. Takamine, M. Kureta, H. Tsutiya, H. Iimura, M. Seya, B. Becker, S. Kopecky, and P. Schillebeeckx, Neutron resonance densitometry for particle-like debris of melted fuel, *Nuclear Data Sheets* **118**, 502 (2014).
 - [16] Y. KUSUMAWATI, I. OZAWA, Y. MITSUYA, T. SHIBA, and M. UESAKA, X-band electron LINAC-based compact neutron source for nuclear debris on-site screening using short-distance neutron resonance transmission analysis, *E-Journal of Advanced Maintenance* **11**, 46 (2019).

- [17] E. M. Engel, E. A. Klein, and A. Danagoulian, Feasibility study of a compact neutron resonance transmission analysis instrument, *AIP Advances* **10**, 015051 (2020), <https://doi.org/10.1063/1.5129961>.
- [18] Y. Podpaly, J. Hall, C. Goyon, P. Kerr, C. Chapman, C. Cooper, J. Mitrani, A. Povilus, B. Shaw, and A. Schmidt, *Environment Insensitive Detection of Fissionable Material with A Short Pulse Neutron Source*, Tech. Rep. (Lawrence Livermore National Lab.(LLNL), Livermore, CA (United States), 2018).
- [19] Starfire Industries, nGen™-400 PORTABLE NEUTRON INTERROGATION, http://www.starfireindustries.com/uploads/2/2/1/1/22111816/datasheet_nngen-400_rev01-19.pdf (2019), last accessed on 06.10.2019.
- [20] J. Lynn, *The Theory of Neutron Resonance Reactions*, International series of monographs on physics (Clarendon P., 1968).
- [21] S. S. M. Wong and S. S. Wong, *Introductory nuclear physics*, Vol. 129 (Wiley Online Library, 1990).
- [22] E. M. Schooneveld, M. Tardocchi, G. Gorini, W. Kockelmann, T. Nakamura, E. Perelli Cippo, H. Postma, N. Rhodes, and P. Schillebeeckx, A new position-sensitive transmission detector for epithermal neutron imaging, *Journal of Physics D: Applied Physics* **42**, 1 (2009).
- [23] A. S. Tremsin, W. B. Feller, and R. G. Downing, Efficiency optimization of microchannel plate (mcp) neutron imaging detectors. I. Square channels with 10B doping, *Nuclear Instruments and Methods in Physics Research Section A: Accelerators, Spectrometers, Detectors and Associated Equipment* **539**, 278 (2005).
- [24] A. Tremsin, T. Shinohara, T. Kai, M. Ooi, T. Kamiyama, Y. Kiyanagi, Y. Shiota, J. McPhate, J. Vallerga, O. Siegmund, and W. Feller, Neutron resonance transmission spectroscopy with high spatial and energy resolution at the J-PARC pulsed neutron source, *Nuclear Instruments and Methods in Physics Research Section A: Accelerators, Spectrometers, Detectors and Associated Equipment* **746**, 47 (2014).
- [25] A. Losko, S. Vogel, M. Bourke, A. Tremsin, A. Favalli, S. Voit, and K. McClellan, Energy-resolved neutron imaging for interrogation of nuclear materials, in *Advances in Nuclear Nonproliferation Technology and Policy Conference* (2016).
- [26] Scintacor, the centre of scintillation, Cambridge CB4 0DL United Kingdom, 6-lithium glass scintillators for neutron detection, <https://scintacor.com/products/6-lithium-glass/>.
- [27] Y. Oshima, T. Yasumune, T. Masuda, K. Maehata, K. Ishibashi, and T. Umeno, Temperature dependence of li-glass scintillator response to neutrons, *Progress in Nuclear Science and Technology* **1**, 296 (2011).
- [28] Z. S. Hartwig, The adaq framework: An integrated toolkit for data acquisition and analysis with real and simulated radiation detectors, *Nuclear Instruments and Methods in Physics Research Section A: Accelerators, Spectrometers, Detectors and Associated Equipment* **815**, 42 (2016).
- [29] R. Brun and F. Rademakers, Root—an object oriented data analysis framework, *Nuclear Instruments and Methods in Physics Research Section A: Accelerators, Spectrometers, Detectors and Associated Equipment* **389**, 81 (1997).
- [30] P. Virtanen, R. Gommers, T. E. Oliphant, M. Haberland, T. Reddy, D. Cournapeau, E. Burovski, P. Peterson, W. Weckesser, J. Bright, S. J. van der Walt, M. Brett, J. Wilson, K. J. Millman, N. Mayorov, A. R. J. Nelson, E. Jones, R. Kern, E. Larson, C. J. Carey, Í. Polat, Y. Feng, E. W. Moore, J. VanderPlas, D. Laxalde, J. Perktold, R. Cimrman, I. Henriksen, E. A. Quintero, C. R. Harris, A. M. Archibald, A. H. Ribeiro, F. Pedregosa, P. van Mulbregt, and SciPy 1.0 Contributors, SciPy 1.0: Fundamental Algorithms for Scientific Computing in Python, *Nature Methods* **17**, 261 (2020).
- [31] Y. Zhang and J.-C. Bilheux, Imagingreso: A tool for neutron resonance imaging, *Journal of Open Source Software* **2** (2017).
- [32] C. A. Wang and R. A. Riedel, *Improved neutron-gamma discrimination for a ⁶Li-glass neutron detector using digital signal analysis methods*, Tech. Rep. (Instrument and Source Division, Neutron Science Directorate, Oak Ridge National Laboratory, Oak Ridge, Tennessee 37831, USA).
- [33] A. Brusegan, G. Noguere, and F. Gunsing, The Resolution Function in Neutron Time-of-Flight Experiments, *Journal of Nuclear Science and Technology* **39**, 685 (2002).
- [34] Thermo Fisher Scientific Inc., MP 320 Neutron Generator, <https://www.thermofisher.com/order/catalog/product/1517021A#/1517021A>.
- [35] D. Brown, M. Chadwick, R. Capote, A. Kahler, A. Trkov, M. Herman, A. Sonzogni, Y. Danon, A. Carlson, M. Dunn, D. Smith, and G. Hale, Endf/b-viii.0: The 8th major release of the nuclear reaction data library with cielo-project cross sections, new standards and thermal scattering data, *Nuclear Data Sheets* **148**, 1 (2018), special Issue on Nuclear Reaction Data.
- [36] D. B. Syme, The black and white filter method for background determination in neutron time-of-flight spectrometry, *Nuclear Instruments and Methods In Physics Research* **198**, 357 (1982).
- [37] J. Hubbell and S. Seltzer, Tables of x-ray mass attenuation coefficients and mass energy-absorption coefficients (version 1.4) (2010).
- [38] P325 Neutron Generator, a compact neutron generator for maximum versatility, http://www.thermo.com.cn/Resources/200802/productPDF_24486.pdf (2019), last accessed on 02.12.2019.
- [39] M. Bourne, C. Mussi, E. Miller, S. Clarke, S. Pozzi, and A. Gueorguiev, Characterization of the clyc detector for neutron and photon detection, *Nuclear Instruments and Methods in Physics Research Section A: Accelerators, Spectrometers, Detectors and Associated Equipment* **736**, 124 (2014).
- [40] N. D'olympia, P. Chowdhury, C. Lister, J. Glodo, R. Hawrami, K. Shah, and U. Shirwadkar, Pulse-shape analysis of clyc for thermal neutrons, fast neutrons, and gamma-rays, *Nuclear Instruments and Methods in Physics Research Section A: Accelerators, Spectrometers, Detectors and Associated Equipment* **714**, 121 (2013).
- [41] G. L. Kulcinski, R. F. Radel, and A. Davis, Near term, low cost, 14mev fusion neutron irradiation facility for testing the viability of fusion structural materials, *Fusion Engineering and Design* **109-111**, 1072 (2016), proceedings of the 12th International Symposium on Fusion Nuclear Technology-12 (ISFNT-12).